

Electronic transport in (La,Sr)MnO₃-ferroelectric-(La,Sr)MnO₃ epitaxial structures

A. G. Boni, I. Pintilie, L. Pintilie, D. Preziosi, H. Deniz et al.

Citation: *J. Appl. Phys.* **113**, 224103 (2013); doi: 10.1063/1.4808335

View online: <http://dx.doi.org/10.1063/1.4808335>

View Table of Contents: <http://jap.aip.org/resource/1/JAPIAU/v113/i22>

Published by the [AIP Publishing LLC](#).

Additional information on J. Appl. Phys.

Journal Homepage: <http://jap.aip.org/>

Journal Information: http://jap.aip.org/about/about_the_journal

Top downloads: http://jap.aip.org/features/most_downloaded

Information for Authors: <http://jap.aip.org/authors>

ADVERTISEMENT



AIP Advances

Now Indexed in
Thomson Reuters
Databases

Explore AIP's open access journal:

- Rapid publication
- Article-level metrics
- Post-publication rating and commenting

Electronic transport in (La,Sr)MnO₃-ferroelectric-(La,Sr)MnO₃ epitaxial structures

A. G. Boni,^{1,2} I. Pintilie,¹ L. Pintilie,¹ D. Preziosi,³ H. Deniz,³ and M. Alexe³

¹National Institute of Materials Physics, Atomistilor 105bis, Magurele 077125, Romania

²University of Bucharest, Faculty of Physics, Magurele 077125, Romania

³Max Planck Institute of Microstructure Physics, Weinberg 2, D-06120, Halle (Saale), Germany

(Received 15 March 2013; accepted 16 May 2013; published online 11 June 2013)

The leakage current in all oxide epitaxial (La,Sr)MnO₃-ferroelectric-(La,Sr)MnO₃ structures, where the ferroelectric layer is either BaTiO₃ or Pb(Zr_{0.2}Ti_{0.8})O₃, was analyzed on a broad range of temperatures and for different thicknesses of the ferroelectric layer. It was found that, although the structures are nominally symmetric, the current-voltage (*I*-*V*) characteristics are asymmetric. The leakage current depends strongly on the thicknesses of the ferroelectric layer, on temperature and on the polarity of the applied voltage. Simple conduction mechanisms such as space charge limited currents or thermionic emission cannot explain in the same time the voltage, temperature, and thickness dependence of the experimentally measured leakage currents. A combination between interface limited charge injection and bulk controlled drift-diffusion (through hopping in the case of BTO and through band mobility in the case of PZT) is qualitatively explaining the experimental *I*-*V* characteristics. © 2013 AIP Publishing LLC. [<http://dx.doi.org/10.1063/1.4808335>]

I. INTRODUCTION

Oxide heterostructures integrating materials with ferromagnetic and ferroelectric properties known as “artificial multiferroics” are of increased interest due to their potential use in microelectronics, sensing, and other high-tech applications.^{1–5} The potential magnetoelectric coupling between the ferromagnetic and ferroelectric phases in multilayer structures opens new possibilities in non-volatile memory devices, as for example multiple states memories or electrical reading of magnetically written information.⁶ Other application, also in the field of non-volatile memories, are based on the simultaneous presence of tunneling magneto-resistance (TMR) and tunneling electro-resistance (TER) in structures combining ferromagnetic oxide electrodes with a ultra-thin ferroelectric layer as conduction barrier.^{7–10} Strontium doped lanthanum manganites La_{1–x}Sr_xMnO₃ (LSMO) are preferred materials in building these artificial layered multiferroics because they have on one side a perovskite structure similar to the main ferroelectric materials such as BaTiO₃ (BTO) and Pb(Zr,Ti)O₃ (PZT) making it appropriate for epitaxial growth and on the other side good magnetic properties at room temperature (RT), its Curie temperature of 350 K being just above RT.^{11,12} LSMO is also known for colossal magnetoresistance thus are good candidates to be used in combination with ferroelectric perovskites for TMR-TER structures or field effect devices.^{13,14} On the other hand, BTO and PZT are prototypical ferroelectric materials with well known ferroelectric properties.^{15–17} Therefore, the combination of LSMO with BTO or PZT in multilayer all oxide heterostructures has a significant potential for applications in microelectronics with special emphasis on non-volatile memories. There are previous studies reporting on LSMO-ferroelectric composites or on LSMO-ferroelectric superlattices or multilayers.^{18–26} However, a detailed study of the leakage current in order to extract information on the possible conduction mechanisms in LSMO-ferroelectric-LSMO

heterostructures has not been yet performed. The current paper presents a detailed analysis of the leakage current in LSMO-ferroelectric-LSMO epitaxial metal-ferroelectric-metal (MFM) structures where the ferroelectric layer was either BTO or PZT. The current-voltage (*I*-*V*) measurements were performed on a broad temperature range and for different thicknesses of the ferroelectric film. It was found that the thickness dependence does not fit with space charge limited currents (SCLC), being both temperature and voltage dependent. Also, the asymmetry of the *I*-*V* characteristics suggests that Pool-Frenkel emission is not an option for the conduction mechanism in LSMO-ferroelectric-LSMO structures. Apparently, the injection into the ferroelectric layer is controlled by the electrode interfaces, but the volume is also playing a role through a combination of SCLC and hopping mechanisms.

II. EXPERIMENTAL METHODS

MFM structures with top and bottom LSMO electrodes were grown by pulsed laser deposition (PLD) on (001)-oriented vicinal SrTiO₃ (STO) substrates with a nominal miscut of 0.1°. First a LSMO layer was deposited on the STO substrate, then the ferroelectric layer and finally the second LSMO layer. The LSMO layers were deposited at 600 °C in oxygen pressure of 0.15 mbar at a laser fluence of about 0.4 J/cm² and repetition rate of 2 Hz. PZT has been grown at 600 °C in oxygen pressure of 0.28 mbar, fluence of about 0.7 J/cm² and 5 Hz repetition rate. BTO has been grown at 650 °C in oxygen pressure of 3 × 10⁻⁵ mbar, fluence of about 1 J/cm² and 5 Hz. All films were cooled from the growth temperature to RT in min. 300 mbar O₂ pressure in order to avoid oxygen non-stoichiometry.

Top Pt contacts of 0.1 mm square were sputtered through a shadow mask. The ferroelectric capacitors with bottom and top LSMO contacts were patterned by etching the top LSMO layer with a diluted solution of sulfuric acid

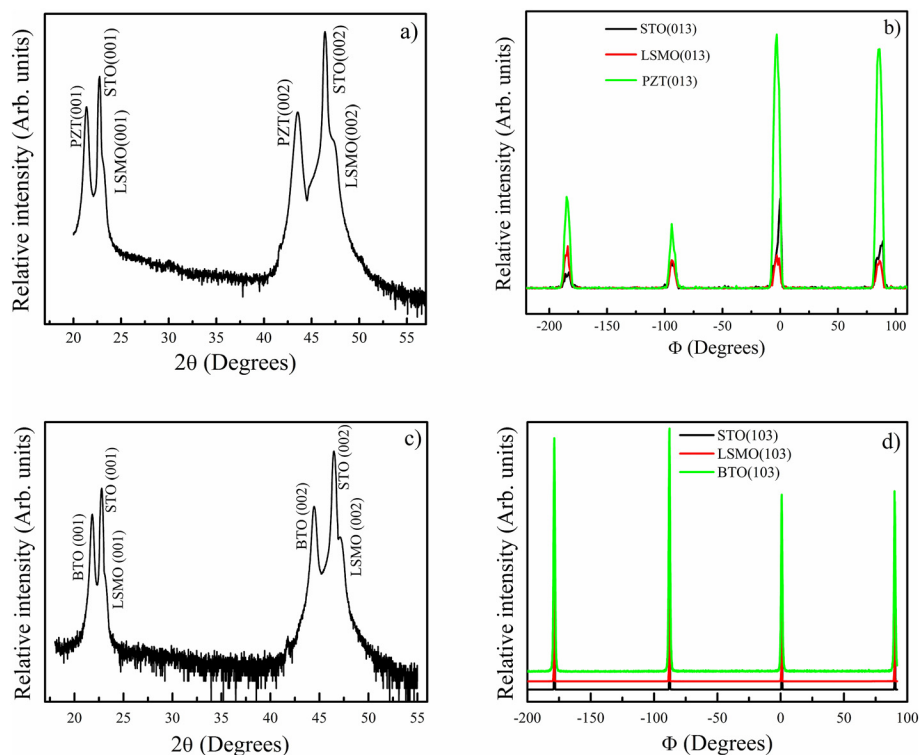


FIG. 1. (a) θ - 2θ scan and (b) ϕ scan of a 100 nm thick PZT layer on LSMO-STO; (c) θ - 2θ scan and (d) ϕ scan of a 90 nm thick BTO layer on LSMO-STO.

and using the Pt contacts as a hard metallic mask. The thickness of the LSMO layers was in all cases of about 25 nm. Different thicknesses were used for the ferroelectric layer: 30 nm and 90 nm for BTO; 25 nm, 50 nm, and 100 nm for PZT. The structural quality of the LSMO-ferroelectric stack was checked by X-ray diffraction and transmission electron microscopy was commonly used to optimize the quality of epitaxial growth and obtain low defect density samples. An example of the typical quality of the layers used in the present study is given in Figure 1 where X-ray data are shown for the LSMO-PZT-LSMO and LSMO-BTO-LSMO cases. Figure 2 shows atomic structure of the PZT-LSMO-STO interfaces. One has to mention that the BTO layer may be fully relaxed, considering that the thickness of the present samples is higher than the critical thickness of 6–7 nm reported in literature.^{27,28}

Current measurements were performed on a large temperature range from 150 K to 400 K by placing the samples

in a LakeShore cryogenic probe station model CPX-VF coupled to a Keithley electrometer model 6517. Ferroelectric properties were evaluated by measuring the hysteresis loop with a ferroelectric tester for thin films model TF2000 (AixaCCt) and by measuring the capacitance-voltage (C-V) characteristic with a HP4194A impedance analyzer.

III. RESULTS AND DISCUSSIONS

A. LSMO-BTO-LSMO structures

Ferroelectric hysteresis measurements performed at different temperatures, shown in Figs. 3(a) and 3(b) for polarization and current, indicate a degradation of the loops with increasing the temperature. This is because of the leakage current, which is increasing with the temperature, especially for the negative polarity, as can be observed in the current hysteresis loops presented in Fig. 3(b). A sharp increase of the current can be seen at 400 K, reflected in the fact that the

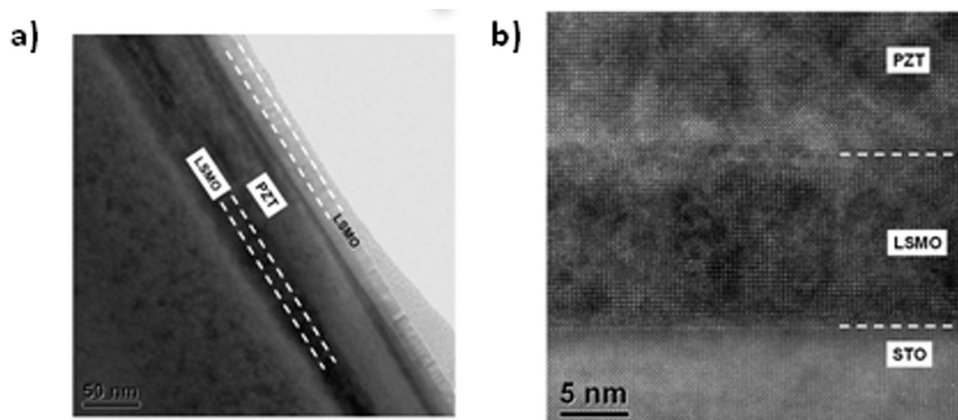


FIG. 2. (a) TEM bright field image of a LSMO-PZT-LSMO heterostructure and (b) high resolution TEM (HRTEM) image of the PZT-LSMO-STO interfaces.

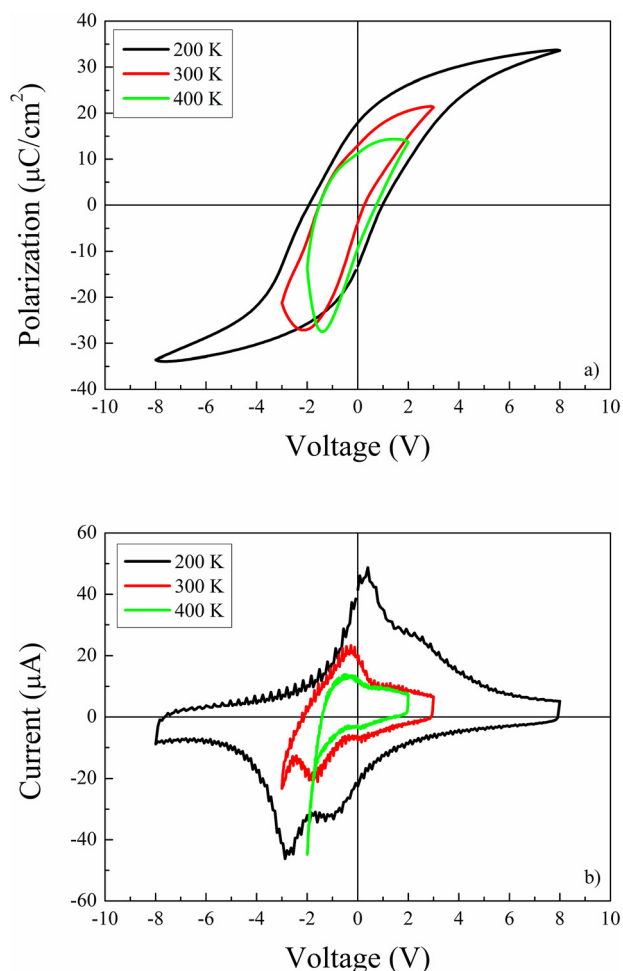


FIG. 3. (a) dielectric hysteresis loop and (b) current hysteresis loop recorded at 1 kHz on LSMO-BaTiO₃-LSMO heterostructure with 30 nm thick BaTiO₃.

saturation regime in the polarization hysteresis could not be achieved at this temperature. Fig. 3(a) shows also that the switching is not sharp, in the sense that the hysteresis loop is far from being rectangular as it should be for a high quality epitaxial film.²⁹ The polarization switching is rather gradual, taking place on a few volts around the coercive field and suggesting the presence of some structural defects acting as pinning centers for the ferroelectric domains. This observation is in agreement with the possible relaxation of the BTO layer, with the formation of structural defects like dislocations, twinning, etc.²⁸ Also, the polarization hysteresis loop is shifted towards negative voltages (reference electrode on top) thus indicating the presence of an internal electric field oriented from top LSMO to bottom LSMO contacts. It might be that there are non-homogeneous distributions of charged defects in the BTO layer, and that the two LSMO-BTO interfaces have dissimilar electronic properties. Even in the case of perfect epitaxial interfaces, the chemical termination of the subsequent layers can induce asymmetries of the interfaces reflected in, for example, offsets of the hysteresis loop.³⁰ The value of the remnant polarization is about $18 \mu\text{C}/\text{cm}^2$, the saturation polarization is about $25 \mu\text{C}/\text{cm}^2$, while the coercive field is about 50 MV/m. I-V characteristics were measured at different temperatures. The current densities for

the samples with different thicknesses of the BaTiO₃ layer were compared at different temperatures (see Fig. 4). At 200 K, the current densities for negative polarities are of comparable values, while for positive polarity the current density is higher for the thinner sample with less than one order of magnitude. Contribution from polarization reversal can be still observed around zero applied bias, up to about 2.5 V, suggesting that the dwell time of 3 s/point was not long enough to eliminate all transient components in the current. However, a longer delay time is detrimental due to gradual breakdown of the contact during repeated I-V measurements. At 300 K, the current densities on positive polarity are about the same, while on the negative polarity the current density is about 40 times larger for the thinner BaTiO₃ film.

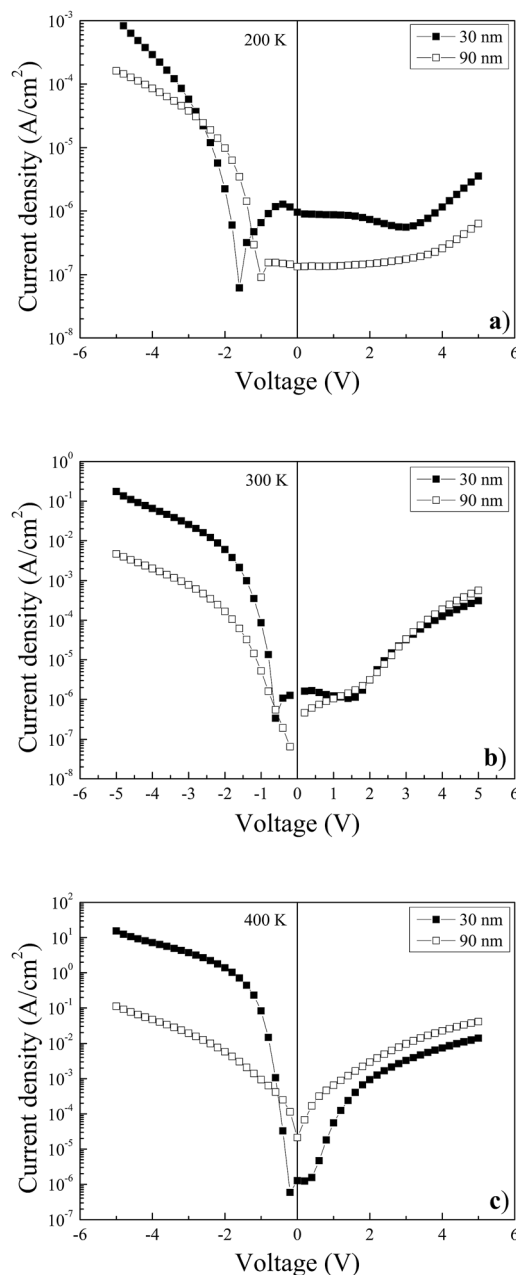


FIG. 4. I-V characteristics of two LSMO-BaTiO₃-LSMO structures, with 30 nm and 90 nm thick BaTiO₃, recorded at (a) 200 K, (b) 300 K, and (c) 400 K.

At 400 K, the current density on negative polarity in the case of the 30 nm thick sample, is about 140 times larger than for the 90 nm thick one. For positive polarity, the situation is reversed and the current density for the 90 nm BaTiO₃ layer is about 4 times larger than for the 30 nm layer.

The asymmetry of the I–V characteristics may suggest that the leakage current is controlled by the interfaces, although the structure is nominally symmetric with bottom and top LSMO electrodes. However, the different deposition sequence for the two interfaces (BaTiO₃ deposited on LSMO for the bottom interface and LSMO deposited on BaTiO₃ for the top interface), as well as the different thermal histories of the two interfaces (the bottom interface experienced high temperatures for a longer time than the top one), can induce different densities of interface states thus different interface electronic properties (barrier height, band bending, etc.). Therefore, a mechanism such as Schottky emission over an interface-located potential barrier seems to be an adequate conduction mechanism to explain the temperature and voltage dependencies of the leakage current.³¹ A more general interface-and-bulk-limited mechanism such as Schottky-Simmons and its associate equation can be used for estimation of the current density taking care that the injection is interface controlled while the drift throughout the film is controlled by the bulk through the pre-exponential mobility term, like in the following equation:^{32,33}

$$J = 2q \left(\frac{2\pi m_{eff} kT}{h^2} \right)^{3/2} \mu E \exp \left(-\frac{q}{kT} \left(\Phi_B^0 - \sqrt{\frac{qE_m}{4\pi\epsilon_0\epsilon_{op}}} \right) \right), \quad (1)$$

where q is the electron charge, h is the Planck's constant, m_{eff} is the effective mass, k is the Boltzmann's constant, μ is the mobility, E is the electric field in the bulk of the ferroelectric, T is the temperature, Φ_B^0 is the potential barrier at zero volts, E_m is the maximum field at the interface if a Schottky-like contact is present (with a depletion region having a voltage dependent width), ϵ_0 is the vacuum permittivity, and ϵ_{op} is the dielectric constant at optical frequencies. Assuming full depletion in BaTiO₃, Eq. (1) can have the following dependency on the thickness d of the ferroelectric layer:

$$J = 2q \left(\frac{2\pi m_{eff} kT}{h^2} \right)^{3/2} \mu \frac{V}{d} \exp \left(-\frac{q}{kT} \left(\Phi_B^0 - \sqrt{\frac{q}{4\pi\epsilon_0\epsilon_{op}}} \frac{V}{d} \right) \right). \quad (2)$$

It is easy to verify that the exponential term does not contribute significantly to the difference in the current densities at different temperatures for the two thicknesses of the BaTiO₃ layer. For example, at +5 V and 200 K, the ratio between the current densities can be as large as 5 for BTO thicknesses of 30 nm and 90 nm, considering a value of 6.5 for the optical dielectric constant. It was assumed that the potential barrier, the mobility, and the effective mass are the same for the samples of different thicknesses of the BaTiO₃ layer. Increasing the temperature, this ratio should decrease, which is confirmed experimentally for the positive side of the I–V

characteristic at 300 K. However, Eq. (2) does not justify the change observed at 400 K, where the current density for 90 nm thick BTO becomes larger than for the thinner film. Also, Eq. (2) does not justify why the ratio of current densities in layers with different thicknesses is larger on the negative polarity compared to the positive polarity.

An increased thickness dependence is given by the SCLC.³⁴ One has to avoid confusion between the space charge region (known also as depletion region) associated with a Schottky contact and the space charge in SCLC mechanism. In the first case, the charge density in the depleted region is uniform and is given by the concentration of the ionized donors and/or acceptors.³⁵ In the second case, the space charge refers to the injected charges into the insulator, when their density becomes larger than the density of the free carriers in the insulator.³⁶ According to the Mott-Gurney law,³⁶ the current density should have a dependence as d^{-3} in this case. For a thickness ratio of 1/3, the ratio of the current densities should be around 30. The problem is that this thickness dependence should not vary with the temperature, meaning that the ratio of the current densities for the two thicknesses of the BaTiO₃ layer should have been about the same at any temperature. However, this is not experimentally observed. On the contrary, Fig. 4 shows that for negative voltage the ratio between current densities increases considerably with temperature, reaching about 140 at 400 K, while for positive voltages the ratio of current densities decreases becoming at 400 K subunitary, meaning that the current is larger in the thicker than in thinner BTO films. Such a behavior cannot be explained with the simple law of the SCLC conduction mechanism.

A steeper dependence on thickness can be obtained in the case of SCLC with an exponential distribution of traps. The current density in this case is given by the following equation:^{37,38}

$$J = q^{1-l} \mu N_c f(l) \left(\frac{\epsilon_0 \epsilon_{st}}{N_t} \right)^l \frac{V^{l+1}}{d^{2l+1}}. \quad (3)$$

Here, N_c is the density of states in the conduction band, assuming that the free carriers are electrons, N_t is the density of traps, ϵ_{st} is the static dielectric constant, d is the film thickness, and $l = T_t/T$ with T_t the characteristic temperature of traps. T_t is related to the activation energy of the traps $E_t = kT_t f(l) = l(2l+1)^{l+1} (l+1)^{-2l-1}$. Therefore, Eq. (3) shows a $J \sim V^m$ dependence on voltage, with $m = l+1$, and a dependence on thickness as d^{-2l-1} . Also, Eq. (3) shows that the current density in this case of SCLC with exponential distribution of traps has a temperature dependence through the quantity l . We have to note here that l normally, should be higher than unity. Deep traps have activation energy E_t higher than 0.1 eV, corresponding to a characteristic temperature of about 1150 K. Considering that current measurements are performed at temperatures of hundreds of K (100–400 K in the present case), it is clear that l should be significantly larger than unity. If $l = 1$, then Eq. (3) transforms in SCLC controlled by shallow traps. Assuming that the quantities μ , N_c , and N_t are the same in the two samples, the value of l can be determined in two ways:

1. By varying the thickness, respectively, at constant temperature and voltage, from the ratio of current densities in the case of two samples with different thicknesses.
2. At constant thickness and temperature, from the $\log J \sim \log V$ representation it is determined the exponent m , and then the quantity l .

The first method is based on the following relation:

$$\frac{J_1}{J_2} = \left(\frac{d_2}{d_1}\right)^{2l+1}, \quad (4)$$

where J_1 and J_2 are the current densities in the samples with thickness d_1 and d_2 , respectively, at the same voltage and temperature. The thickness ratio will be the same at any voltage and temperatures. In principle, the quantity T_i should be also the same, although small variations of the activation energy are possible with temperature and voltage. Therefore, the quantity l should decrease with increasing the temperature. Assuming that $d_1 < d_2$, the term in the right hand side of Eq. (4) should decrease with increasing the temperature, thus the ratio of current densities J_1/J_2 should also decrease with increasing the temperature. In our specific case on the negative polarity of the I–V characteristics, the ratio of the current densities is actually increasing with the temperature. On the positive side, the temperature dependence is even more complicated, starting with a higher than unity ratio at 200 K and ending with a lower than unity ratio at 400 K. Equations (3) and (4) cannot explain thus the experimental results.

Just for completeness of the analysis, the second method to determine l was also tested. The $\log J \sim \log V$ representation at different temperatures is shown in Fig. 5.

Figure 5 shows a “normal” behavior for SCLC with exponential distribution of traps. A steep increase of the current can be observed in the I–V characteristic at any temperature. The voltage range where this increase occurs is dependent on temperature. This behavior corresponds to the trap-filling regime. After the steep increase, the voltage dependence goes to V^2 , corresponding to the trap-free SCLC regime. This one should be temperature independent. The lines in Fig. 5 show that indeed there is a convergence of the I–V

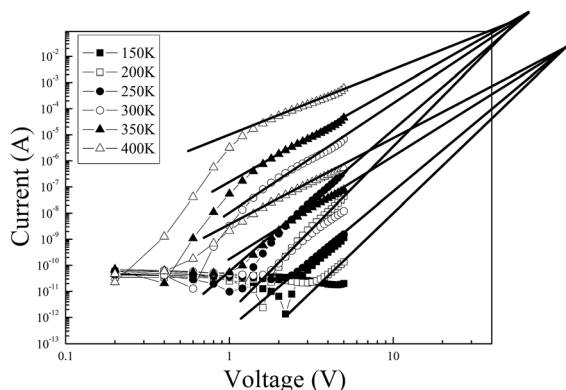


FIG. 5. The $\log J \sim \log V$ representation at different temperatures for the LSMO-BaTiO₃-LSMO structures with 30 nm thick BaTiO₃. The higher currents are for the negative bias. The lines are guide for the eye showing the convergence to the temperature independent SCLC trap free regime.

characteristics towards a “cross-over” point which is reached at about 60 V for the negative polarity and at about 100 V for the positive polarity.

The parameter l , calculated from the slope of the steeper part of the I–V characteristics at 400 K for the negative polarity, is 8, leading to a characteristic temperature of 3200 K and an activation energy of about 0.28 eV. About the same values were obtained for 350 K and 300 K. On the positive polarity, the l value is about 6, leading to an activation energy of about 0.2 eV. Therefore, it can be claimed that there are two exponential distributions of traps, located near the electrode interfaces, and that they have different activation energies because the processing conditions for the two interfaces were different.

The above paragraph and discussion shows how false conclusions can be drawn if measurements are performed only on one thickness. In the present case, having two samples with very different thicknesses it is easy to argue, based on the results presented in Fig. 4, that the SCLC with exponential distribution of traps is not the right conduction mechanism to explain the experimental I–V characteristics. In fact, the above considerations based on the thickness dependence of the current density lead to the conclusion that SCLC can be ruled out as the main conduction mechanism in the studied samples.

The most puzzling result is the increase of the leakage by increasing the film thickness, see Fig. 4(c) in the positive polarity. The only conduction mechanism at which the current density increases with the volume of the sample is hopping conduction.^{39,40} On the other hand, the strong asymmetry of the I–V characteristics and the temperature dependence suggest an additional interface controlled carrier injection mechanism, most probably Schottky emission. Therefore, we propose a conduction mechanism based on interface controlled charge injection into the BaTiO₃ layer, and a bulk controlled drift by a thermally activated hopping mechanism. In the followings, we present a detailed analysis in the case of the 30 nm thick BTO film.

The temperature dependence of the electric conductivity in the case of thermally activated hopping is given by⁴¹

$$\sigma \sim T^{-3/2} \exp\left(-\frac{W_a}{kT}\right), \quad (5)$$

where W_a is the activation energy for hopping. It can be observed that the temperature dependence is similar to the one of the Schottky-Simmons in Eq. (1). Arrhenius plots for several voltages are shown in Fig. 6. It can be easily seen from the slopes of the linear fit in Fig. 6 that the estimated activation energy W_a of the hopping mechanism is obviously voltage dependent. Bearing in mind that the carrier injection is controlled by interfaces through thermionic emission, a $V^{1/2}$ dependence was tested for the activation energy. The plot W_a vs. $V^{1/2}$ is shown in Fig. 7. The $V^{1/2}$ dependence of the activation energy is confirmed, supporting thus the initial assumption that the carriers are injected by thermionic emission into the ferroelectric BaTiO₃ layer. The barriers at zero bias are about 0.51 eV for positive polarity and about 0.74 eV for negative bias. However, the fact that the activation energy is

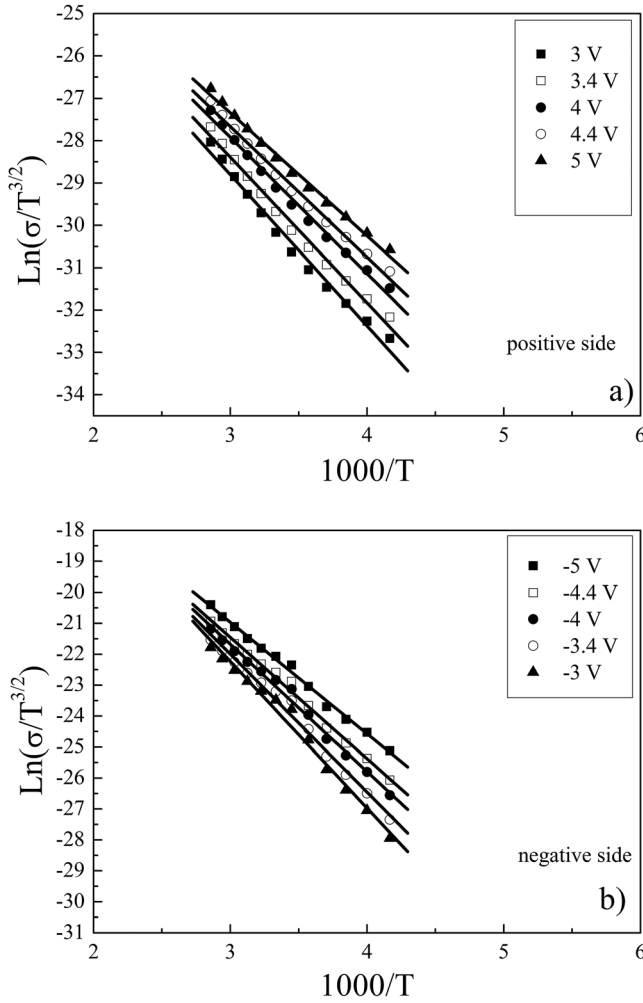


FIG. 6. Arrhenius plots for several voltages on both positive and negative sides of the I-V characteristics. The lines are the linear fits.

higher on the negative polarization is in contradiction with the experimental data, which show higher currents for negative polarity (see Fig. 4). Therefore, the temperature dependence predicted by Eq. (6) may not be entirely correct, at least for the negative polarity.

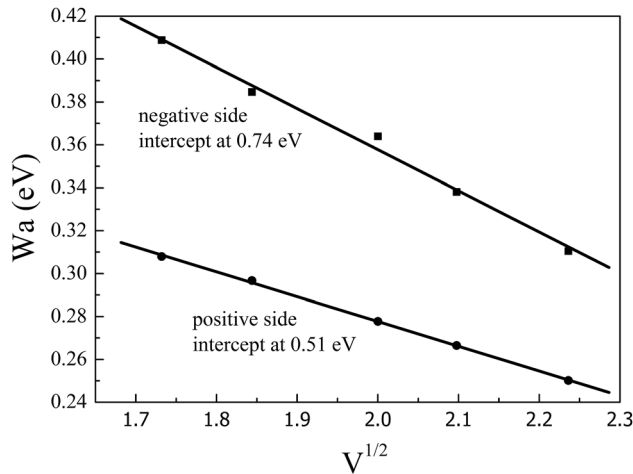


FIG. 7. The voltage dependence of the activation energy for negative and positive polarities of the I-V characteristics for a LSMO-BTO (30 nm)/LSMO heterostructure. The lines are the linear fits.

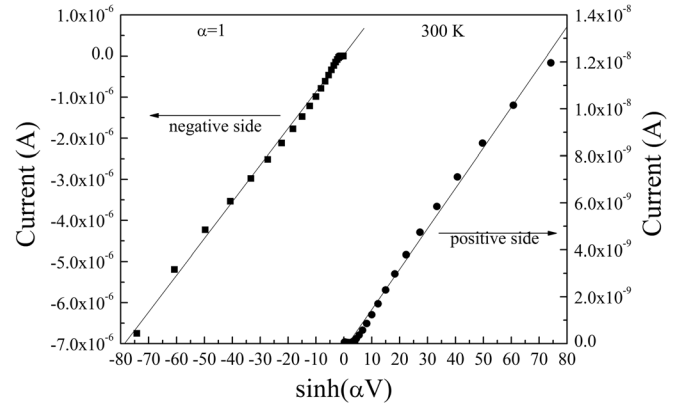


FIG. 8. The representation of the measured current as function of $\sinh(\alpha V)$ for a constant temperature of 300 K.

Another aspect which must be considered is the strong nonlinearity of the I-V characteristics. In the case of the thermally activated hopping, the voltage non-linearity is explained by the following equation:⁴¹

$$j \sim \sinh\left(\frac{Vqa}{2kT_w}\right) \exp\left(-\frac{W_a}{kT}\right). \quad (6)$$

Here, w is width of the high resistance region of the film, assimilated to the depletion region of a Schottky type contact, and a is the distance between two neighboring hopping sites. In order to prove the dependence shown in Eq. (6), the current at a temperature of 300 K was represented as function of $\sinh(\alpha V)$ where the quantity $\alpha = qa/2kT_w$ (see Fig. 8).

A linear dependence of the measured current on $\sinh(\alpha V)$ is obtained. The value estimated for α from the linear fit is 1 for both polarities. Assuming a hopping distance of about 4 nm, which represents a concentration of the hopping sites of one at approximately 10 unit cells similar to the oxygen vacancies concentration of about 10^{19} cm^{-3} , a normal value in ferroelectric perovskites,⁴²⁻⁴⁴ a value of about 70 nm is obtained for w . w is larger than the film thickness, suggesting that even at zero volts the BaTiO₃ film is fully depleted and thus the electric field inside the film can be simply calculated as V/d .

Considering the above discussion, the following equation, which combines both thermionic emission and hopping conduction, is proposed for explaining the temperature and voltage dependence of the current density in the studied LSMO-BTO-LSMO structures:

$$J_{+/-} = F_1(E_a - / + E_i) \exp\left(-\frac{q}{kT} \left((\Phi_B^0 + W_a) - \sqrt{\frac{q(E_a - / + E_i)}{4\pi\epsilon_0\epsilon_{op}}} \right)\right). \quad (7)$$

Here, E_a is the applied field, and E_i is the internal (imprint) field whose presence is suggested by the hysteresis measurements shown in Fig. 3. The \pm signs stand for the positive and negative polarities. The term $W_a + \Phi_B^0$ takes into consideration the thermal activation energy (the potential barrier)

for the hopping and the height of the potential barrier (at zero field) for the thermionic emission. The pre-exponential term may have temperature and voltage dependence, and may include also the mobility of the charge carriers. However, for the present simulations, it will be considered that this term is constant with electric field, temperature, and thickness. Fig. 9 shows simulated I–V characteristics for three temperatures together with the experimental data. The simulations were performed according to Eq. (7) and using: a pre-exponential factor of 10^{-2} A; a value of 0.51 ± 0.05 eV for the quantity $W_a + \Phi_B^0$ in the case of the positive polarity; an internal (imprint) field produced by a voltage of 1 V (as suggested by the hysteresis loop in Fig. 3) and oriented from top to bottom electrode; a value of about 6 for the optical dielectric constant;⁴⁵ and a thickness of 30 nm for the BaTiO₃ layer. On the negative polarity, the simulation was performed using the following values for the quantity

$W_a + \Phi_B^0$; 0.39 eV at 200 K; 0.36 eV at 300 K; 0.28 eV at 400 K.

It can be seen that Eq. (7) simulates quite well the experimental I–V characteristics. On the positive side, it seems that the total activation energy for conduction, given by the sum between the interface barrier and activation energy of the hopping conduction $W_a + \Phi_B^0$ does not vary with the temperature, suggesting negligible effect from the interface states. On the negative side, the total activation energy $W_a + \Phi_B^0$ decreases with increasing the temperature, most probably because of the potential barrier associated with the electrode interface Φ_B^0 . This is possible when interface traps, which show temperature dependent occupation state, are involved in lowering the effective barrier besides the changes induced by the inherent asymmetry of the interfaces. The thickness dependence of Eq. (7) was also verified. The results are presented in Fig. 10 for the temperature of 400 K and two thicknesses of the BTO film, i.e., 30 nm and 90 nm.

It is clear that Eq. (7) cannot fully describe the thickness dependence, although on the negative side this dependence is correctly simulated at least qualitatively. It may be that microstructural defects such as misfit dislocations or oxygen vacancies can distort the simple thickness dependencies of the conduction mechanisms used to explain the experimental data, dependencies which were deduced assuming homogeneous properties of the film over the entire volume.

In conclusion, the conduction mechanism in LSMO-BaTiO₃-LSMO epitaxial structures was investigated and it was found that:

1. The conduction mechanism is a combination between thermionic injection controlled by the potential barriers associated to electrode interfaces and thermally activated hopping;
2. Oxygen vacancies may be involved in the hopping mechanism. Also, their non-uniform distribution may explain the presence of the internal field and the different potential barriers at the two electrode interfaces as well as complex thickness dependence.

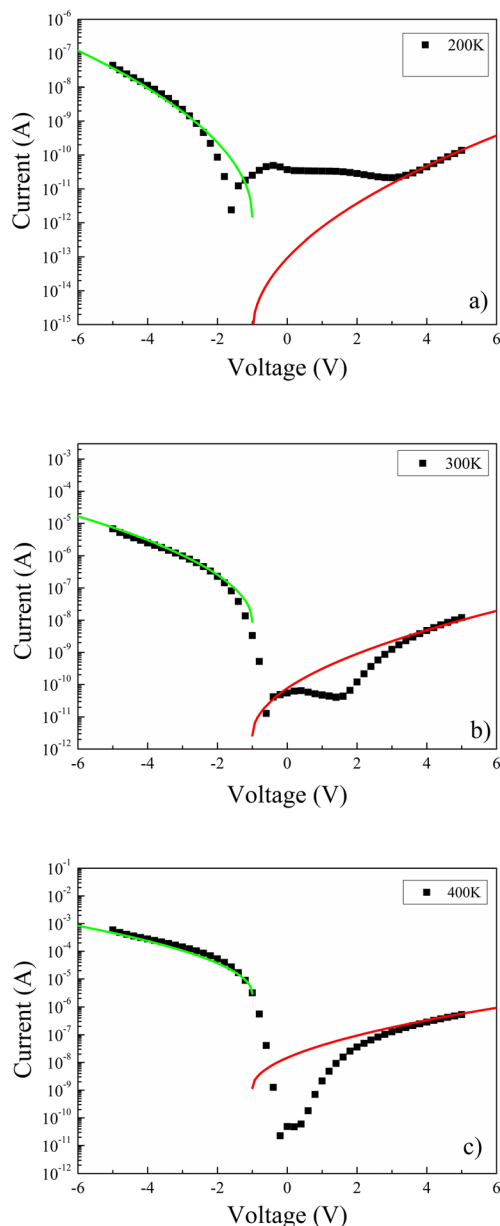


FIG. 9. Experimental and simulated I–V characteristics at three temperatures: (a) 200 K; (b) 300 K; (c) 400 K.

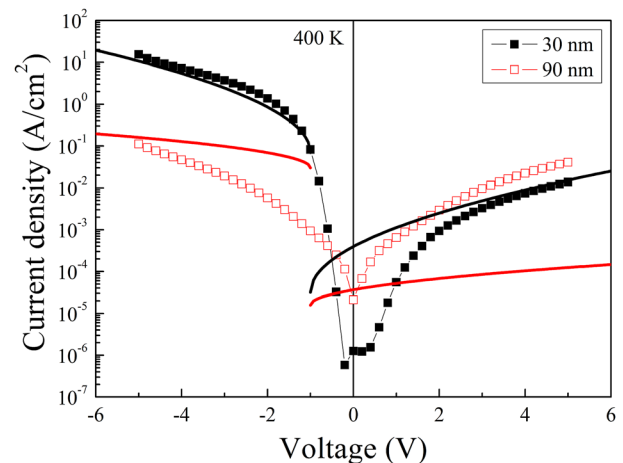


FIG. 10. Experimental (symbols) and the simulated (lines) I–V characteristics, respectively, for heterostructures with 30 nm and 90 nm BTO layer thicknesses.

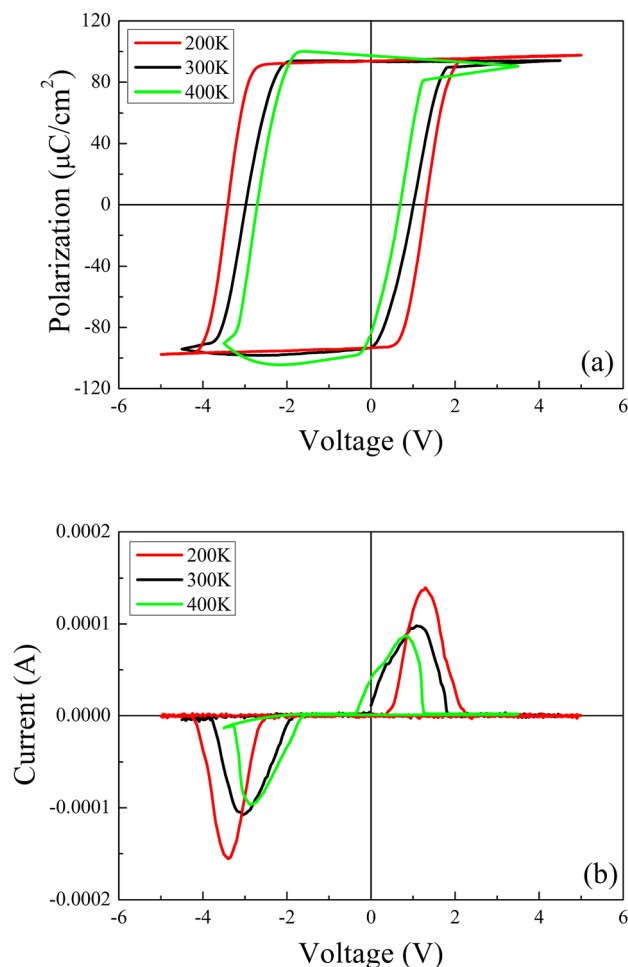


FIG. 11. Ferroelectric hysteresis loop (a) and the corresponding current hysteresis loop (b) recorded at different temperatures for a LSMO-PZT-LSMO heterostructure with 100 nm thick PZT.

B. LSMO-PZT-LSMO structures

In order to verify the generality of the above conduction mechanism, we have applied the concept to a similar structure, but with different ferroelectric layer. We have grown all epitaxial LSMO-PZT-LSMO heterostructures and we have applied similar analysis as for the heterostructures with BTO.

The ferroelectric properties were also checked by measuring the hysteresis loop at different temperatures. The obtained results are shown in Fig. 11. Compared to the case of LSMO-BTO-LSMO structures, the magnitude of the ferroelectric polarization is much higher, reaching nearly $100 \mu\text{C}/\text{cm}^2$.⁴⁶ The hysteresis is almost rectangular, with a strong imprint towards negative voltages. The imprint is similar to the BTO case suggesting thus a common origin. The coercive field is of about 20 MV/m.

I–V characteristics at room temperature and for different thicknesses are presented in Fig. 12. It can be seen that these are strongly asymmetric, with different thickness dependences for the two voltage polarities.

Referring to Fig. 12, it can be seen that on the positive bias the magnitude of the current increases with the thickness. The ratio of the current values for 25 nm and 100 nm

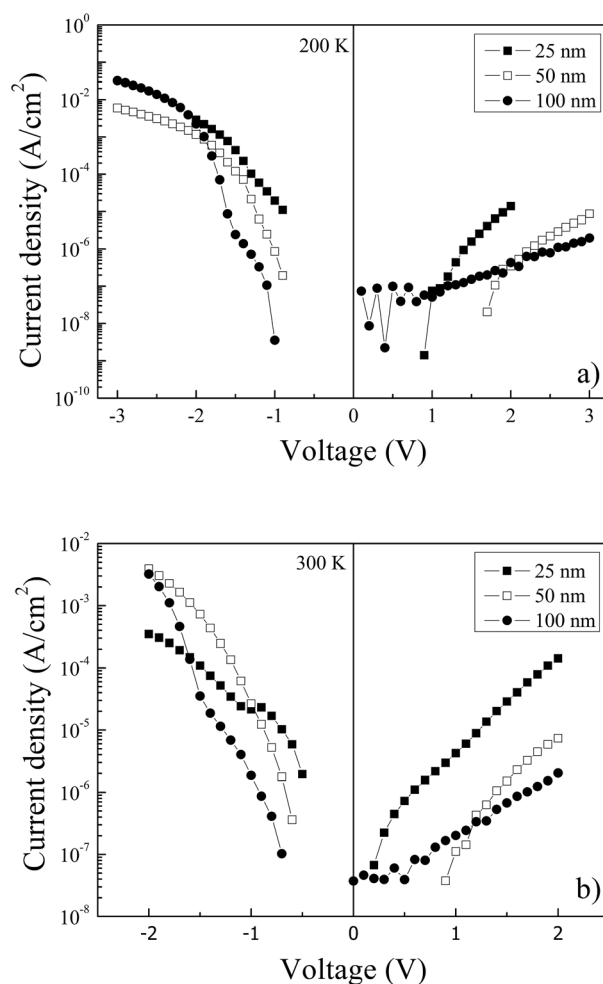


FIG. 12. I–V characteristics measured at (a) 200 K and (b) 300 K on LSMO-PZT-LSMO structures with 25 nm, 50 nm, and 100 nm thick PZT layer.

thick PZT films, at a voltage of 2 V is about 70 at 300 K and about 40 at 200 K, suggesting SCLC as conduction mechanism. We remind here that in the case of SCLC the current decreases as d^{-3} , with d the thickness of the film, thus the current should decrease 64 times for the 100 nm thick film compared to the 25 nm thick PZT. Therefore, the ratios between 40 and 70 are close to the theoretical value of 64. However, on the negative bias, the current increases with increasing thickness up to about 1 V, then the thickness dependence becomes quite complicated, with no clear trend. An increase of the current with thickness suggests a hopping mechanism, as discussed for the case of LSMO-BTO-LSMO structures.

Further on, similar to Figure 4 in the case of the BTO-based structures, we have represented the I–V characteristics at different temperatures in log-log scale (see Fig. 13). It can be seen that for negative bias the current has the tendency to become temperature independent at voltages over 2 V, corresponding to SCLC with exponential distribution of traps (the discussion referring to Figure 5 in Sec. III A). For positive polarity (Fig. 13(b)), the current increases with the temperature but the slope in the log-log plot seems to be constant. This fact may be possible for SCLC with a shallow distribution of traps³⁶

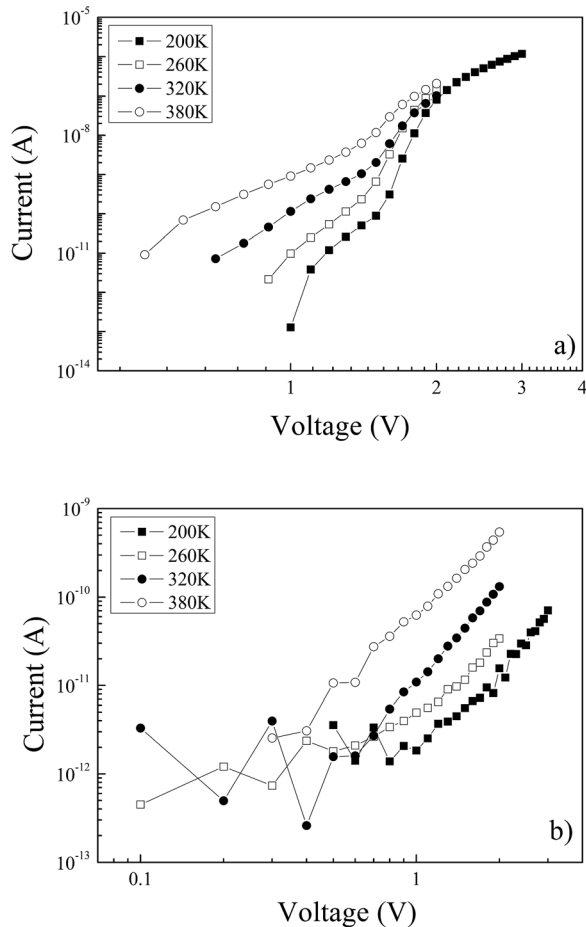


FIG. 13. The $\log J \sim \log V$ representations for (a) negative and (b) positive fields, respectively, and at different temperatures for the 100 nm thick PZT layer.

$$J = \frac{9}{8} \epsilon_0 \epsilon_{st} \mu \theta \frac{V^2}{d^3}. \quad (8)$$

The only difference compared to the trap free regime is the term θ , which is the ratio of the free carriers to the trapped carriers. θ has a temperature dependence proportional with $\exp(-E_t/kT)$, where E_t is the activation energy of the trapping level. Therefore, increasing T leads to an increase of the current because the value of θ is increasing (more free /less trapped carriers). Indeed, representing $\text{Ln}(\text{Current}) \sim 1000/T$ for a voltage of 2 V an Arrhenius type plot is obtained. An activation energy of about 0.15 eV is obtained from the slope of this plot (see Fig. 14).

However, the slope of the log-log I-V representation in Fig. 13, for positive bias, is around 3 at all temperatures, suggesting a double injection SCLC.³⁶ In this case, the thickness dependence should be as d^{-5} , which is not experimentally confirmed. All in all, the analysis performed on the experimental data considering SCLC as dominant conduction mechanism leads to contradictory results, so, as in the BTO case, the SCLC alone cannot explain the experimental findings.

We have thus performed analysis similar to the case of LSMO-BTO-LSMO structures in order to estimate the potential barriers at the two electrode interfaces. The following values were found:

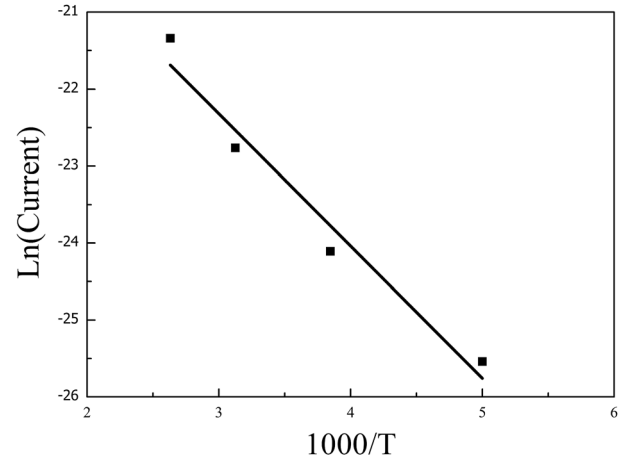


FIG. 14. Arrhenius plot for a positive bias of 2 V. The line represents the linear fit.

1. 0.45 ± 0.05 eV for both voltage polarities in the case of the PZT layer with 25 nm thickness
2. 0.45 ± 0.05 eV for positive voltage and 0.75 ± 0.05 eV for negative voltage in the case of the PZT layer with 50 nm thickness
3. 0.25 ± 0.05 eV for positive voltage and 0.8 ± 0.05 eV for negative voltage in the case of the PZT layer with 100 nm thickness

As for BTO, the potential barrier is constantly lower for the positive bias. The values are quite similar, which is a very interesting result considering that the two ferroelectric materials have significantly different remnant polarization and dielectric constant. Considering that the trend of the I-V characteristics with voltage, thickness, and temperature is similar to those analyzed in detail for LSMO-BTO-LSMO structure, one can think that the conduction mechanism is also similar; respectively, a combination of interface controlled injection and volume controlled hopping. However, in the case of the LSMO-PZT-LSMO structures, Eq. (6) does not hold in the sense that the current does not have a linear dependence on $\sinh(\alpha V)$ for both polarities and with the same value for α as was found for the BTO-based structures. It results that in the case of the PZT the conduction mechanism is similar to the one reported in Ref. 32, with interface controlled injection and bulk controlled drift-diffusion through the mobility term in Eq. (1).

IV. CONCLUSIONS

The leakage current in epitaxial LSMO-ferroelectric-LSMO heterostructures, where the ferroelectric layer is either BTO or PZT, was studied over a broad temperature range and for different thicknesses of the ferroelectric layer. The thickness dependence is different for different voltage and temperature domains and does not fit simple SCLC model. The asymmetry of the I-V characteristics and the voltage square root dependence of the activation energies suggest both interface and bulk controlled conduction mechanisms. A combination of thermionic injection and thermally activated hopping is the closest to explain the voltage and

temperature dependence, but fails to explain the thickness dependence for the LSMO-BTO-LSMO structure. Similar experimental results are obtained for the LSMO-PZT-LSMO heterostructures. The conduction mechanism in latter case seems to be a combination between thermionic injection at the electrode interface and bulk controlled drift-diffusion through the band mobility of the injected carriers. Further experimental and theoretical studies are needed in order to clarify the origin of the charge transport in artificial type multiferroic structures based on LSMO and ferroelectric layers.

ACKNOWLEDGMENTS

The work was performed in the frame of the FP7 IFOX project (Grant No. 246102). The Romanian team acknowledges also some financial support from the Project PN-II-ID-PCCE-2011-2-0006 (Contract No. 3/2012).

- ¹L. W. Martin, S. P. Crane, Y. H. Chu, M. B. Holcomb, M. Gajek, M. Huijben, C. H. Yang, N. Balke, and R. Ramesh, *J. Phys.: Condens. Matter* **20**, 434220 (2008).
- ²J. Ma, J. Hu, Z. Li, and C. W. Nan, *Adv. Mater.* **23**, 1062 (2011).
- ³C. W. Nan, M. I. Bichurin, S. Dong, D. Viehland, and G. Srinivasan, *J. Appl. Phys.* **103**, 031101 (2008).
- ⁴R. Ramesh and N. A. Spaldin, *Nature Mater.* **6**, 21 (2007).
- ⁵D. I. Khomskii, *Physics* **2**, 20 (2009).
- ⁶J. F. Scott, *Nature Mater.* **6**, 256 (2007).
- ⁷Y. W. Yin, M. Raju, W. J. Hu, X. J. Weng, X. G. Li, and Q. Li, *J. Appl. Phys.* **109**, 07D915 (2011).
- ⁸M. Ye. Zhuravlev, S. Maekawa, and E. Y. Tsymbal, *Phys. Rev. B* **81**, 104419 (2010).
- ⁹D. Pantel, S. Goetze, D. Hesse, and M. Alexe, *Nature Mater.* **11**, 289 (2012).
- ¹⁰D. Pantel, S. Goetze, D. Hesse, and M. Alexe, *ACS Nano* **5**, 6032 (2011).
- ¹¹Z. Trajanovic, C. Kwon, M. C. Robson, K.-C. Kim, M. Rajeswari, R. Ramesh, T. Venkatesan, S. E. Lofland, S. M. Bhagat, and D. Fork, *Appl. Phys. Lett.* **69**, 1005 (1996).
- ¹²P. Perna, C. Rodrigo, E. Jiménez, F. J. Teran, N. Mikuszeit, L. Méchin, J. Camarero, and R. Miranda, *J. Appl. Phys.* **110**, 013919 (2011).
- ¹³R. Mundle, R. B. Konda, O. Bamiduro, O. Yasar, F. Williams, M. Bahoura, A. K. Pradhan, D. R. Sahu, J.-L. Huang, and D. E. Nikonov, *J. Appl. Phys.* **105**, 07C907 (2009).
- ¹⁴C. A. F. Vaz, J. Hoffman, Y. Segal, J. W. Reiner, R. D. Grober, Z. Zhang, C. H. Ahn, and F. J. Walker, *Phys. Rev. Lett.* **104**, 127202 (2010).
- ¹⁵M. E. Lines and A. M. Glass, *Principles and Applications of Ferroelectrics and Related Materials* (Clarendon Press, Oxford, UK, 1977).
- ¹⁶M. Klee, F. L. Eusemann, F. L. Waser, W. Brand, and H. van Hal, *J. Appl. Phys.* **72**, 1566 (1992).
- ¹⁷M. de Keijsers, J. F. M. Cillessen, R. B. F. Janssen, A. E. M. De Veirman, and D. M. de Leeuw, *J. Appl. Phys.* **79**, 393 (1996).
- ¹⁸Y. P. Lee, S. Y. Park, Y. H. Hyun, J. B. Kim, V. G. Prokhorov, V. A. Komashko, and V. L. Svetchnikov, *Phys. Rev. B* **73**, 224413 (2006).
- ¹⁹R. Martínez, A. Kumar, R. Palai, R. S. Katiyar, and J. F. Scott, *J. Appl. Phys.* **107**, 114107 (2010).
- ²⁰M. Sirena, E. Kaul, M. B. Pedreros, C. A. Rodriguez, J. Guimpel, and L. B. Steren, *J. Appl. Phys.* **109**, 123920 (2011).
- ²¹V. G. Prokhorov, V. A. Komashko, G. G. Kaminsky, K. K. Yu, S. J. Jun, S. Y. Park, J. S. Park, Y. P. Lee, and V. L. Svetchnikov, *Low Temp. Phys.* **33**, 58 (2007).
- ²²P. S. Krishnan, M. Arredondo, M. Saunders, Q. M. Ramasse, N. Valanoor, and P. Munroe, *J. Appl. Phys.* **109**, 034103 (2011).
- ²³W. Wu, K. H. Wong, C. L. Choy, and Y. H. Zhang, *Appl. Phys. Lett.* **77**, 3441 (2000).
- ²⁴F. Chen, Q. Z. Liu, H. F. Wang, F. H. Zhang, and W. Wu, *Appl. Phys. Lett.* **90**, 192907 (2007).
- ²⁵J. Hoffman, X. Hong, and C. H. Ahn, *Nanotechnology* **22**, 254014 (2011).
- ²⁶D. Mukherjee, R. Hyde, M. Hordagoda, N. Bingham, H. Srikanth, S. Witanachchi, and P. Mukherjee, *J. Appl. Phys.* **112**, 064101 (2012).
- ²⁷G. Niu, B. Gautier, S. Yin, G. Saint-Girons, P. Lecoeur, V. Pillard, G. Hollinger, and B. Vilquin, *Thin Solid Films* **520**, 4595 (2012).
- ²⁸J. Q. He, E. Vasco, R. Dittmann, and R. H. Wang, *Phys. Rev. B* **73**, 125413 (2006).
- ²⁹A. Petraru, N. A. Pertsev, H. Kohlstedt, U. Poppe, A. Solbach, U. Klemradt, and R. Waser, *J. Appl. Phys.* **101**, 114106 (2007).
- ³⁰H. Lu, X. Liu, J. D. Burton, C.-W. Bark, Y. Wang, Y. Zhang, D. J. Kim, A. Stamm, P. Lukashev, D. A. Felker, C. M. Folkman, P. Gao, M. S. Rzechowski, X. Q. Pan, C.-B. Eom, E. Y. Tsymbal, and A. Gruverman, *Adv. Mater.* **24**, 1209 (2012).
- ³¹W. Schottky, *Phys. Z.* **41**, 570 (1940).
- ³²J. G. Simmons, *Phys. Rev. Lett.* **23**, 297 (1969).
- ³³L. Pintilie, I. Vrejoiu, D. Hesse, G. LeRhun, and M. Alexe, *Phys. Rev. B* **75**, 104103 (2007).
- ³⁴K. C. Kao and W. Hwang, *Electrical Transport in Solids* (Pergamon, Oxford, 1981).
- ³⁵S. M. Sze, *Physics of Semiconductor Devices* (Wiley, New York, 1981).
- ³⁶M. A. Lampert and P. Mark, *Current Injection in Solids* (Academic, New York, 1970).
- ³⁷D. S. Shang, L. D. Chen, Q. Wang, W. Q. Zhang, Z. H. Wu, and X. M. Li, *Appl. Phys. Lett.* **89**, 172102 (2006).
- ³⁸V. Kumar, S. C. Jain, A. K. Kapoor, J. Poortmans, and R. Mertens, *J. Appl. Phys.* **94**, 1283 (2003).
- ³⁹J. Rybickiy, A. Rybickay, S. Feliziani, and M. Chybicki, *J. Phys.: Condens. Matter* **8**, 2089 (1996).
- ⁴⁰M. L. Knotek, M. Pollak, T. M. Donovan, and H. Kurtzman, *Phys. Rev. Lett.* **30**, 853 (1973).
- ⁴¹U. Boettger and V. Bryskin, *Hopping Conduction in Solids* (Akademie Verlag, Berlin, 1985).
- ⁴²L. Pintilie, I. Boerasu, M. J. M. Gomes, T. Zhao, R. Ramesh, and M. Alexe, *J. Appl. Phys.* **98**, 124104 (2005).
- ⁴³C. S. Hwang, B. T. Lee, C. S. Kang, K. H. Lee, H. J. Cho, H. Hideki, W. D. Kim, S. I. Lee, and M. Y. Lee, *J. Appl. Phys.* **85**, 287 (1999).
- ⁴⁴M. Dawber and J. F. Scott, *Appl. Phys. Lett.* **76**, 1060 (2000).
- ⁴⁵W. Kinase, J. Kobayashi, and N. Yamada, *Phys. Rev.* **116**, 348 (1959).
- ⁴⁶I. Vrejoiu, G. Le Rhun, L. Pintilie, D. Hesse, M. Alexe, and U. Gösele, *Adv. Mater.* **18**, 1657 (2006).